

1 **Title:**

2 **Development of a Bespoke Finite Element Wear Algorithm to Investigate the Effect of**
3 **Femoral Centre of Rotation on the Wear Evolution in Total Knee Replacements**

4 **Authors:**

5 **Ciaran Neil Pitt^{a,*}, Ariyan Ashkanfar^a, Russell English^a, Andrew Naylor^a, Tahsin T. Öpöz^a, David J.**
6 **Langton^b, Thomas J. Joyce^c**

7 *a. School of Engineering, Liverpool John Moores University, Byrom Street, Liverpool, L3 3AF, UK*

8 *b. ExplantLab, Newcastle Upon Tyne, NE4 5BX, UK*

9 *c. School of Engineering, Newcastle University, Newcastle Upon Tyne, NE1 7RU, UK*

10 **Keywords:**

11 Wear modelling, Total knee replacement, Finite element modelling, Polyethylene wear, Femoral wear

12 **Abstract**

13 Total Knee Replacements (TKRs) are a commonly used treatment to help patients suffering from
14 severely damaged knee joints, which is normally brought on by osteoarthritis. The aim of the surgery
15 is to reduce pain and regain function of the joint, however, some of these implants fail prematurely
16 with implant wear being one of the main factors of failure. Computational analysis is an efficient tool
17 that can provide an in-depth insight on the evolution of wear, before utilising experimental techniques
18 which are time-consuming and costly. In this study, a bespoke finite element (FE) based wear
19 algorithm has been further developed for TKRs and was used to investigate how location of femoral
20 centre of rotation (CoR) affects the evolution of wear at the bearing surfaces. Three locations of
21 femoral CoR have been investigated: international standards (ISO) CoR, being the location defined in
22 ISO 14243-3, distal CoR being the centre of the femoral component's distal radius, and reference CoR
23 being the middle ground between the two. All investigations were setup in accordance with ISO
24 14243-3 for displacement-controlled wear testing conditions for knee simulators. The wear algorithm
25 extracts contact pressure and sliding distance from the FE analysis to determine wear depth, wear
26 pattern, volumetric wear, and wear rates on the polymeric insert and femoral component's bearing
27 surfaces using Archard's wear law. The polymeric insert volumetric wear rate after 5 million cycles
28 (Mc) for ISO, reference, and distal CoR are 4.37mm³/Mc, 5.40mm³/Mc, and 6.83mm³/Mc respectively.
29 Furthermore, the wear pattern's location on the bearing surfaces is dependent on the femoral CoR,
30 with ISO CoR wear pattern being positioned more posteriorly, distal CoR being more anteriorly, and
31 reference CoR in between ISO and distal. The ISO CoR investigation showed a region of minimal wear
32 between two wear regions at the middle of the femoral component's wear pattern, on both medial
33 and lateral condyles. This region of minimal wear reduces for the reference CoR and further reduces
34 for the distal CoR. After 5 Mc, the average polymeric insert-femoral component contact area changes
35 with femoral CoR, with the average contact area being 66.53mm², 68.35mm², and 71.21mm² for ISO,
36 reference, and distal CoRs respectively, with distal having around 7% more contact area than ISO. The
37 results from this study show that there is a wide range of wear values for different locations of femoral
38 CoR. As such the choice of femoral CoR should be carefully considered when performing any wear
39 investigation to ensure that the CoR location is consistent for all studies being compared.

* Corresponding author.

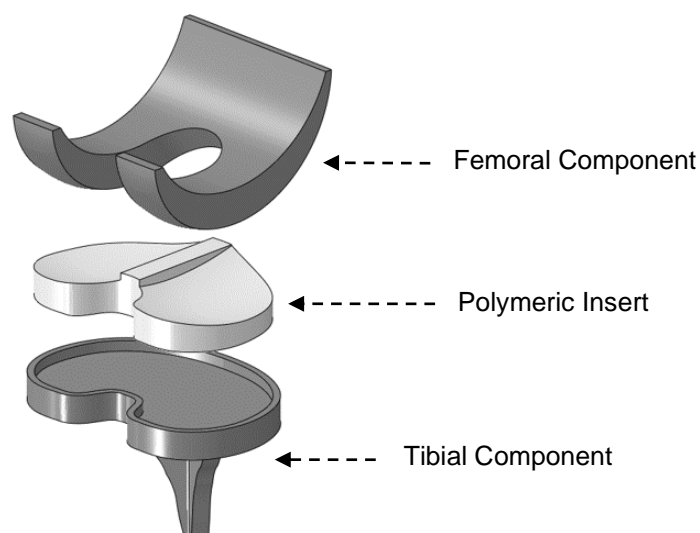
E-mail address: c.n.pitt@2016.ljmu.ac.uk, cnp967@gmail.com (C.N. Pitt).

40 1. Introduction

41 The knee joint is the largest and one of the most complex weight bearing joints in the human body.
42 Many factors can damage the joint, diseases such as osteoarthritis cause pain and loss of mobility or
43 function of the joint (Michael, Schlüter-Brust and Eysel, 2010). For cases when initial treatments such
44 as exercise and painkillers fail to alleviate pain (Michael, Schlüter-Brust and Eysel, 2010; Jevsevar,
45 2013; Skou et al., 2018), joint-preserving surgery such as arthroscopy debridement is performed to
46 smoothen and remove damaged cartilage and clean up meniscal damage (Michael, Schlüter-Brust and
47 Eysel, 2010). However, for late-stage osteoarthritis, knee arthroplasty is required to replace the
48 damaged knee joint with either a unicompartmental (partial) or a total knee replacement (TKR) (Beard
49 et al., 2019).

50 The National Joint Registry (NJR) annual report in 2023, which covers England, Wales, Northern
51 Ireland, the Isle of Man and Guernsey, states that since 2003 there has been over 1,540,000 primary
52 knee replacements implanted, and over the last three years the number of primary knee procedures
53 implanted from 2020-2022 was over 232,500 (NJR, 2023). In this period over 198,500 are primary
54 TKRs, with the average age of implantation being around 70 years old (NJR, 2023). Hence TKRs are
55 the most common procedure to treat knee joints with end-stage knee osteoarthritis (Carr et al., 2012;
56 Gao et al., 2020).

57 A commercial TKR typically comprises of the femoral component, polymeric insert, and tibial
58 component, shown in Figure 1. The femoral component is primarily manufactured from cobalt
59 chromium (CoCr) (Wright-Walker and LaBerge, 2013; Hussain, Saleem and Ahmad, 2019), the
60 polymeric insert traditionally from ultra-high molecular weight polyethylene (UHMWPE) but more
61 recently cross-linked polyethylene (XLPE) is also used (Wright-Walker and LaBerge, 2013; Chacko
62 Rajan et al., 2020), and the tibial component from a titanium alloy (Ti-6Al-4V) (Wright-Walker and
63 LaBerge, 2013; Hussain, Saleem and Ahmad, 2019).



64

65

Figure 1 - Fundamental Components of a TKR

66 In 2014, it was interpreted that approximately 90% of TKRs will last around 13 to 14 years (Castagnini
67 et al., 2017), and in 2019, around 82% will last 25 years (Evans et al., 2019), however, younger active
68 patients (≤ 65 years old) are receiving TKRs more frequently over the last decade (Bayliss et al., 2017;

69 Witjes et al., 2017; Price et al., 2018). This is a cause for concern since younger patients are at higher
70 risk of revision surgery (Julin et al., 2010; Bayliss et al., 2017; Castagnini et al., 2017; Price et al., 2018;
71 NJR, 2023), and should only receive TKRs in exceptional circumstances (Julin et al., 2010). This
72 highlights the importance to reduce failure rates and improve the survivability of TKRs.

73 Over the last decade, there is evidence that TKRs have failed prematurely (Scholes et al., 2013; Drohat,
74 Kiehl and Mess, 2018; Bhalekar et al., 2021). Implants can fail in many different ways, hence eight
75 modes of failure have been defined by Vince (2014): infection, extensor mechanism deficiency,
76 stiffness, instability, patellar maltracking, aseptic loosening and osteolysis, periprosthetic fracture, and
77 component breakage. Studies have been performed to investigate the main factors for TKR failure, as
78 such, Kim et al. (2014) highlighted that the three major causes were polyethylene (PE) wear (44.1%),
79 infection (38.7%), and aseptic/component loosening (12.1%). More recently, the NJR (2023) reported
80 that aseptic loosening (31.8%), progressive arthritis (21.1%), instability (17.0%), and implant wear
81 (13.8%) were the main reason for knee revision surgery over the last 5 years. It should be noted that
82 factors such as aseptic/component loosening and instability can occur due to PE wear induced
83 osteolysis (Kandahari et al., 2016). As such, it can be seen that wear, in particular PE wear, is one of
84 the main limiting factors on the survivability of TKRs. Wear can be investigated by experimental
85 techniques, such as knee simulators, which can be costly and time consuming (Fitzpatrick et al., 2016;
86 Kang et al., 2017), or computational analysis which offers a less expensive, quick and effective solution
87 to investigate TKR wear (Knowlton et al., 2020).

88 Knee simulator wear testing is usually setup in accordance with international standards, either ISO
89 14243-1 (2009) or ISO 14243-3 (2014), force or displacement controlled respectively (Maag et al.,
90 2021; Abdelgaied, Fisher and Jennings, 2022). The ISO standard specifies a goal of reaching at least 5
91 million cycles (Mc), where 1 Mc can be considered to be equivalent of around one year of a patient
92 walking (Schmalzried et al., 1998). In addition, the standard specifies the location of femoral centre of
93 rotation (CoR), however there are discrepancies in application of femoral CoR, with some studies using
94 a location determined by the ISO standard, and others using the centre of the distal radius (Brockett
95 et al., 2016; Abdelgaied, Fisher and Jennings, 2022). This discrepancy on femoral CoR location provides
96 a change in where the femoral component will articulate across the bearing surface of the polymeric
97 insert, and thus the pressure distribution and consequently the wear evolution is affected.

98 Previously wear has been predicted for total hip replacements (THRs) through the development of a
99 bespoke FE wear algorithm to predict fretting wear (English, Ashkanfar and Rothwell, 2015), and more
100 recently bearing surface wear (Toh et al., 2021). In this study, the FE wear algorithm has been further
101 developed to predict bearing surface wear on a TKR model using Archard's wear law (Archard and
102 Hirst, 1956), in an FE package Abaqus (2019, Abaqus Inc). In addition, an investigation on both PE
103 wear, which has been widely investigated computationally (Fregly et al., 2005; Abdelgaied et al., 2011;
104 Mell et al., 2018; Wang et al., 2019; Koh et al., 2020), and femoral component wear, which has not
105 been widely recognised in the literature has been performed. Although the amount of metallic wear
106 may be minimal for TKRs, metal debris is dangerous and may lead to serious complications such as
107 metallosis (Willis-Owen, Keene and Oakeshott, 2011). The aim of this study is to determine how the
108 location of femoral CoR, affects the wear on both the polymeric insert and femoral component's
109 bearing surface (PE-CoCr bearing surface) over 5 million walking cycles.

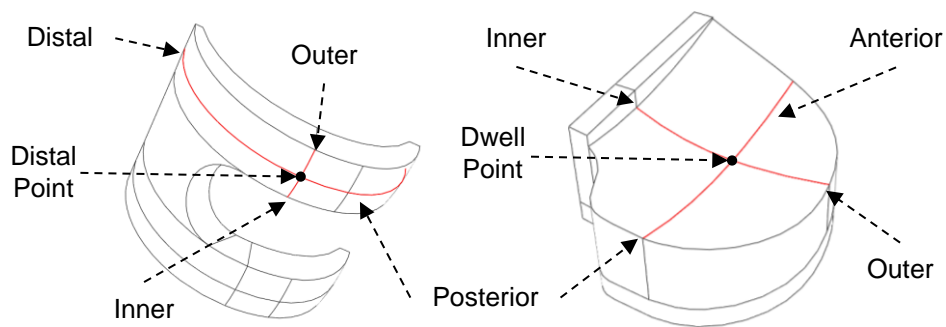
110 2. Methodology

111 The method employed in this study utilised our bespoke FE wear algorithm (English, Ashkanfar and
112 Rothwell, 2015; Toh et al., 2021), which has been further developed using Python programming to

113 incorporate Archard’s wear law, which is a widely used method to simulate wear for TKRs (Knight et
 114 al., 2007; O’Brien et al., 2013; Willing, 2013; Wang et al., 2018; Ozer, 2022). The algorithm predicts
 115 wear at each point of contact between the PE-CoCr bearing surface by extracting contact pressures
 116 and sliding distances throughout a walking cycle, to calculate wear using the wear law.

117 2.1. Finite Element Modelling

118 The femoral, and polymeric insert/tibial component of a right TKR has been modelled in Abaqus,
 119 shown in Figure 2. The components have dimensions assigned to four radii, the anterior (distal for
 120 femoral component), posterior, inner, and outer radii, which are based on a commercial TKR (Walker,
 121 Lowry and Kumar, 2014), shown in Figure 2. The anterior radius has not been included for the femoral
 122 component as this radius would not have any contact on the PE-CoCr bearing surface. The components
 123 have an approximate sizing of around a femoral size = ‘E’ (approx. anterior-posterior length = 62mm,
 124 medial-lateral length = 72mm), and tibial size = ‘4’ (approx. anterior-posterior length = 46mm, medial-
 125 lateral length = 70mm), as per commercial sizing for TKRs, which varies with manufacturers. A J-Curve
 126 design for the femoral component has been used, which is a two radii design (Pfitzner et al., 2018).
 127 The medial and lateral side of both the polymeric insert and femoral components are symmetrical,
 128 which is the case for most commercial designs (Walker, 2015; Pfitzner et al., 2018) and the material
 129 properties assigned to each component are shown in Table 1.



130

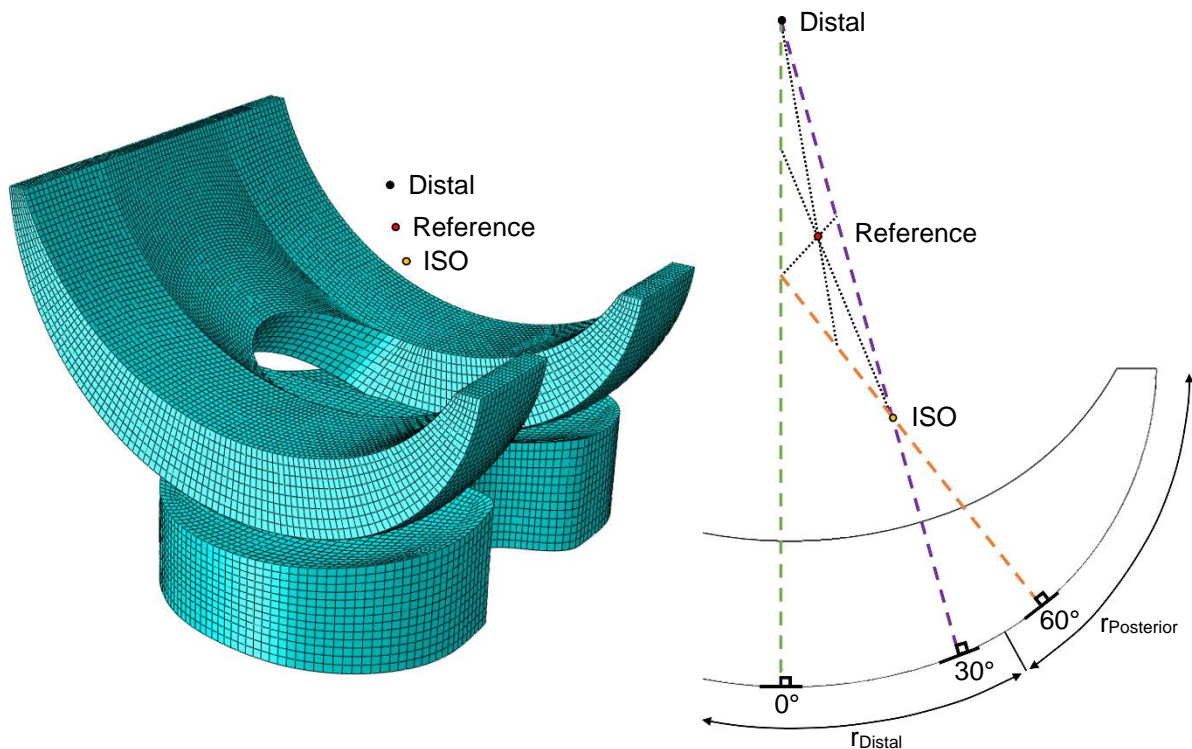
131 *Figure 2 – Creation of Components: Femoral (Left), Half Model of Polymeric Insert/Tibial Component (Right)*

Component (Material)	Young’s Modulus [GPa]	Poisson’s Ratio	Density [kg/m ³]
Femoral (CoCr)	220	0.30	7800
Polymeric Insert (PE)	0.91	0.46	930
Tibial (Ti-6Al-4V)	109	0.33	4430

132

Table 1 - Material Properties for FE Components

133 The components were assembled in accordance with ISO 14243-3 (2014), hence that the bottom of
 134 each femoral condyle, the distal point, sits coincident with the dwell point, the lowest point of the
 135 polymeric insert’s bearing surface, as indicated in Figure 2. The assembly of the components is shown
 136 in Figure 3. A mesh convergence study has been performed for the FE model, and the converged mesh
 137 consisted of hexahedral 8-node linear, with reduced integration elements (C3D8R), with an
 138 approximate element mesh size of 1mm for each component, shown in Figure 3.



139

140 *Figure 3 - Assembly of TKR & Converged Mesh (Left) & Creation of The Three CoRs – Femoral Component Side View, Angles*
 141 *and Radii Annotations are for Illustration Purposes and Not to Scale (Right)*

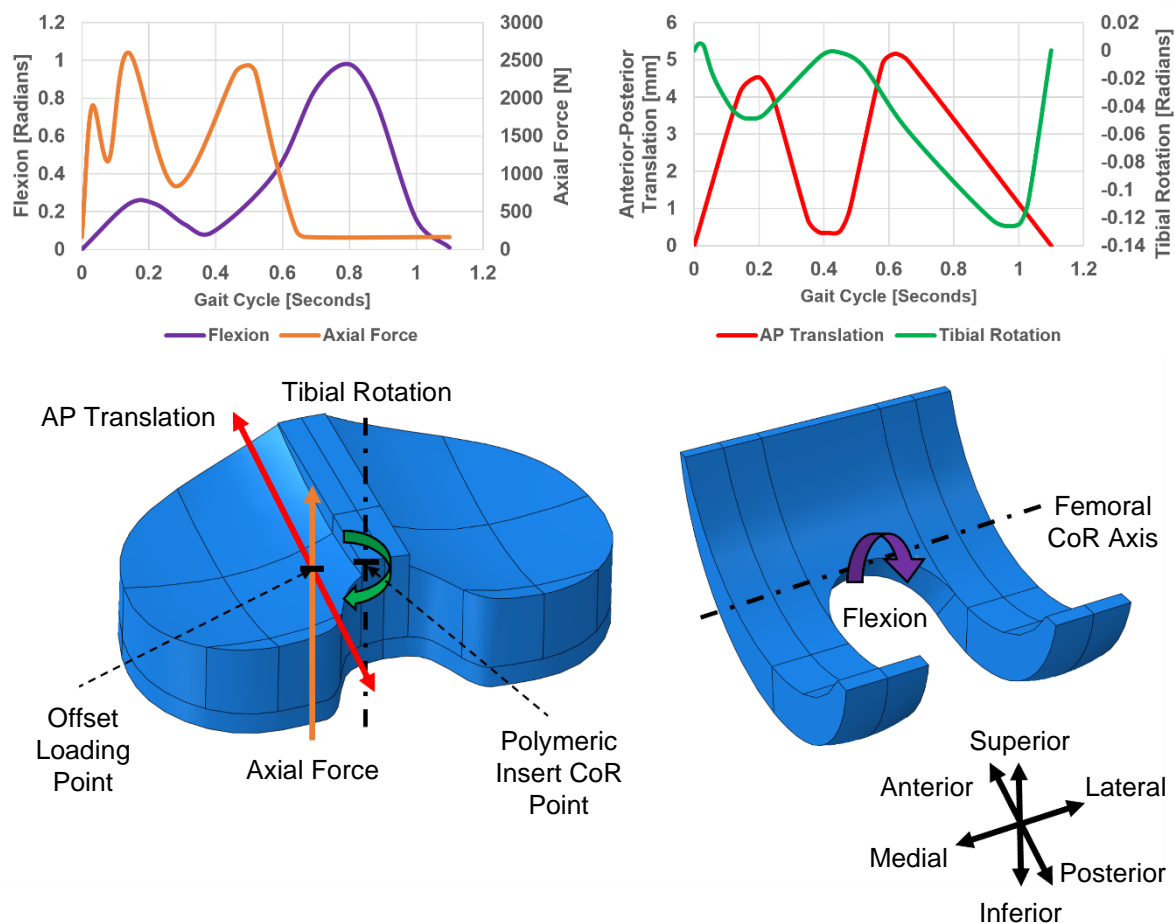
142 Three different investigations for the location of femoral CoR have been included in this study, ISO
 143 (yellow dot), distal (black dot), and reference (red dot) CoR, as defined by Mell, Wimmer and Lundberg
 144 (2019), shown in Figure 3. The ISO CoR is applied as described in the ISO 14243-3 (2014) standard for
 145 knee simulators, where an imaginary contact plane at 30° (purple) and 60° (orange) flexion at the
 146 femoral bearing surface has a contact normal line. The point where the two imaginary contact normal
 147 lines (purple and orange) cross determines the location of the ISO CoR. The distal CoR being the centre
 148 of the circle of the distal radius, and the reference CoR being the centre of the triangle that is formed
 149 from the three lines (green, purple, and orange) used for the creation of the other two points. The
 150 creation of the three CoRs are shown in Figure 3.

151 The ISO 14243-3 (2014) contains the following gait cycles: flexion, axial force, anterior-posterior (AP)
 152 translation, and tibial rotation, Figure 4. These cycles allow the FE model to have the motion and
 153 loading of a walking cycle on a level surface. For each investigation, these gait cycles with loading and
 154 boundary conditions are assigned to each component in accordance with the displacement-controlled
 155 ISO 14243-3 (2014), with the only variation being the location of femoral CoR for the reference and
 156 distal CoR investigations. A dynamic implicit analysis over a 1.1 second time period, in accordance with
 157 ISO 14243-3 (2014), has been set up, with an incrementation set to 20 evenly spaced increments over
 158 the cycle. This incrementation ensures that all the loading and rotational characteristics of the gait
 159 cycles (Figure 4) are accounted for in the FE analysis.

160 The PE-CoCr bearing surface interaction has been defined in Abaqus as a surface to surface contact
 161 employing a ‘penalty’ method with a coefficient of friction of 0.04 (Ozer, 2022). For the FE model to
 162 be able to simulate a right TKR walking, points were created to assign the gait cycles to the
 163 components: polymeric insert CoR and offset loading point, and the chosen femoral CoR which is on
 164 the femoral CoR axis, shown in Figure 4. The femoral CoR point was coupled to the proximal surface

165 of the femoral component. The polymeric insert offset loading point is offset medially from the centre
 166 by 0.07 times the width of the polymeric insert (4.87mm), as defined by ISO 14243-3 (2014); and was
 167 coupled to the distal surface of the polymeric insert. The polymeric insert CoR point, is located at
 168 distal-centre surface of the polymeric insert, which was coupled to the medial-lateral surface that
 169 connects the proximal and distal surfaces.

170 The femoral component was only allowed to rotate around the femoral CoR axis (medial-lateral),
 171 whereas the tibial component was restricted from rotating around the medial-lateral axis, but was
 172 free to move in all other directions (Mell, Wimmer and Lundberg, 2019; Wang et al., 2019). Flexion
 173 gait cycle was applied at the femoral CoR, while the axial force was assigned to the offset loading point
 174 in the superior-inferior axis, this simulates the body weight acting more so on the inside of the joint
 175 (Knight et al., 2007; Wang et al., 2018). On this offset loading point, the AP translation gait cycle
 176 was applied along the AP axis, whereas the tibial rotation was applied to the polymeric insert CoR point in
 177 the superior-inferior axis. The assignment of gait cycles for the femoral component and polymeric insert
 178 insert are shown in Figure 4.



179

180

Figure 4 - ISO Gait Cycle Data (Top) & Assignment of Gait Cycles on FE Model (Bottom)

181 **2.2. Computational Wear Modelling**

182 In this study, our previously validated bespoke FE wear algorithm for investigating wear using
 183 Dissipated Energy wear law on THRs (English, Ashkanfar and Rothwell, 2015; Toh et al., 2021), has
 184 been further developed in order to investigate wear for the complex geometry of TKRs using Archard's
 185 wear law. According to Archard's wear law (Archard and Hirst, 1956) the volumetric wear, W_{Vol} , can

186 be calculated for the contacting surfaces by the product of wear coefficient, K , contact force, F , and
 187 a sliding distance, s , shown in Equation (1).

$$W_{Vol} = KFs \quad (1)$$

188 As such linear wear depth, W_D , for each point at the contacting surface, can be calculated using
 189 Equation (2), where P is the contact pressure at the interaction surfaces.

$$W_D = KPs \quad (2)$$

190 For the wear depth to be accurately modelled in the FE analysis for a walking cycle, it is necessary to
 191 calculate the wear at each time interval, i , of the gait cycle for a total number of time intervals, n . As
 192 such the cyclic wear depth, W_{Dc} , is calculated using Equation (3), where \bar{P}_i and Δs_i are the contact
 193 pressure and sliding distance at a specific time interval, i .

$$W_{Dc} = \sum_{i=1}^n K\bar{P}_i\Delta s_i \quad (3)$$

194 To replicate the ISO standard of 5 Mc, a “scaling factor” (β) is introduced so that the wear analysis is
 195 completed in an effective and efficient manner. β represents a specific number of walking cycles,
 196 which scales the wear depth calculated by the chosen value, so that the analysis is computationally
 197 efficient. Hence for this study, total wear depth, W_{Dt} , generated over a specified total number of
 198 walking cycles, N , is calculated using Equation (4), where j represents a specific “analysis stage”
 199 reflecting the evolution of wear.

$$W_{Dt} = \sum_{j=1}^{(N/\beta)} \beta \sum_{i=1}^n K\bar{P}_i\Delta s_i \quad (4)$$

200 The value of β must be investigated via a convergence study to ensure the accuracy of the wear is not
 201 compromised (English, Ashkanfar and Rothwell, 2015). The value for β used in literature varies from
 202 50,000 (Kang et al., 2017; Koh et al., 2020) to 500,000 cycles (Knight et al., 2007; Abdelgaied et al.,
 203 2011; Mell et al., 2018; Abdelgaied, Fisher and Jennings, 2022). A β convergence study was performed
 204 for our model to calculate accurate results efficiently. This resulted in a β value of 100,000, a smaller
 205 value such as 50,000 would double the computational runtime for 2% more volumetric wear accuracy
 206 every 1Mc, which is not computationally viable.

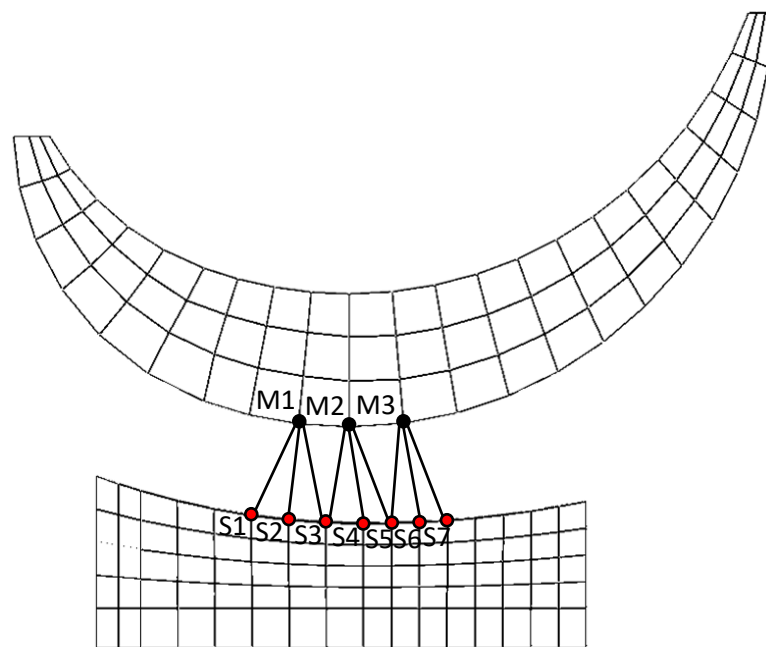
207 After creating the FE model and assigning loading and boundary conditions, an FE input file is written
 208 to be used within the wear algorithm. The wear analysis study requires the interacting surfaces, wear
 209 fraction, wear law, wear coefficient, β value, and number of wear cycles, which are shown in Table 2.

Wear Algorithm Input:	Description:
Interacting Surfaces	PE-CoCr Bearing Surface
Wear Fraction	0.99:0.01 (PE:CoCr)
Wear Law	Archard’s Wear Law
Wear Coefficient	2.64E-07mm ³ /Nm
Scaling Factor (β)	100,000
Number of Wear Cycles	50

Table 2 - Wear Algorithm Input Parameters

211 The algorithm extracts the normal direction for each node on the PE-CoCr bearing surface, so that
212 there is a direction to apply wear depth for each node in contact. To calculate wear depth at the
213 surface interaction, nodes on the femoral bearing surface must be paired with nodes on the polymeric
214 insert bearing surface through a “pairing” command of the algorithm (English, Ashkanfar and
215 Rothwell, 2015; Toh et al., 2021). This command has been further developed to be compatible with
216 the more complicated TKR geometry. Due to the complexity of the TKR geometry, and different mesh
217 densities, a 1-1 pairing technique as demonstrated by English, Ashkanfar and Rothwell (2015) would
218 not be suitable. The pairing command determines which nodes of the polymeric insert and femoral
219 bearing surfaces are the closest to each other, and then pairs 1 node of the femoral bearing surface,
220 that has a slightly coarser mesh, to 3 nodes of the polymeric insert’s bearing surface, which has a
221 slightly finer mesh, for each increment of the cycle. This method is essential for the TKR model to
222 ensure that all the nodes in contact on the PE-CoCr bearing surface are being paired. A simplified 2D
223 representation of the 1-3 “pairing nodes” technique is shown in Figure 5. For instance, pairing 1 will
224 have a wear depth that is the average of femoral node M1, being paired to the three polymeric insert
225 nodes S1, S2, and S3, whereas pairing 2 will have a wear depth that is the average of node M2 being
226 paired to the three nodes S3, S4, and S5 and similarly for pairing 3. For nodes which are shared
227 between pairings, such as S3 in this case, the wear depth would be an average of the wear depth of
228 pairing 1 and 2. Due to the small size of the elements, this averaging will not affect the accuracy of the
229 wear depth results or the wear pattern.

230 A portion of the wear depth calculated is then applied to each node in the pairings using a “wear
231 fraction”, which for this study is 0.99:0.01 for PE:CoCr. The value of wear fraction has been calculated
232 by analysing the gravimetric release of PE and the plasma-mass spectrometry of metallic debris for
233 each material during a wear test by Kretzer et al. (2014).



234

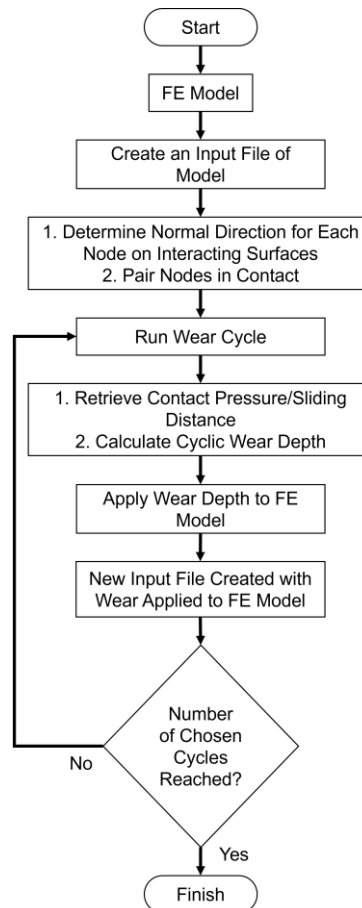
235

Figure 5 – 1-3 Pairing Nodes Technique - 2D Representation

236 Contact pressures and sliding distances are extracted for each time interval of the cycle for the paired
237 nodes, which is used to calculate the wear depth using Equation (4), with the wear coefficient being
238 $2.64E-07\text{mm}^3/\text{Nm}$ (Knight et al., 2007; Wang et al., 2018; Lee, Kim and Lim, 2022). The subsequent
239 wear depth calculated is then applied to the relevant nodes in the normal direction of the surface by

240 updating the nodes coordinates, so that the next cycle has the geometrical changes applied to the FE
241 model. This procedure is demonstrated in the flowchart (Figure 6) and is further explained by English,
242 Ashkanfar and Rothwell (2015) and Toh et al. (2021). All analysis in this study was performed using a
243 workstation with 128GBs RAM and 24 Core at 3.79GHz, which completes a 5 Mc analysis using a β
244 value of 100,000 (50 analysis), in around 123 hours.

245



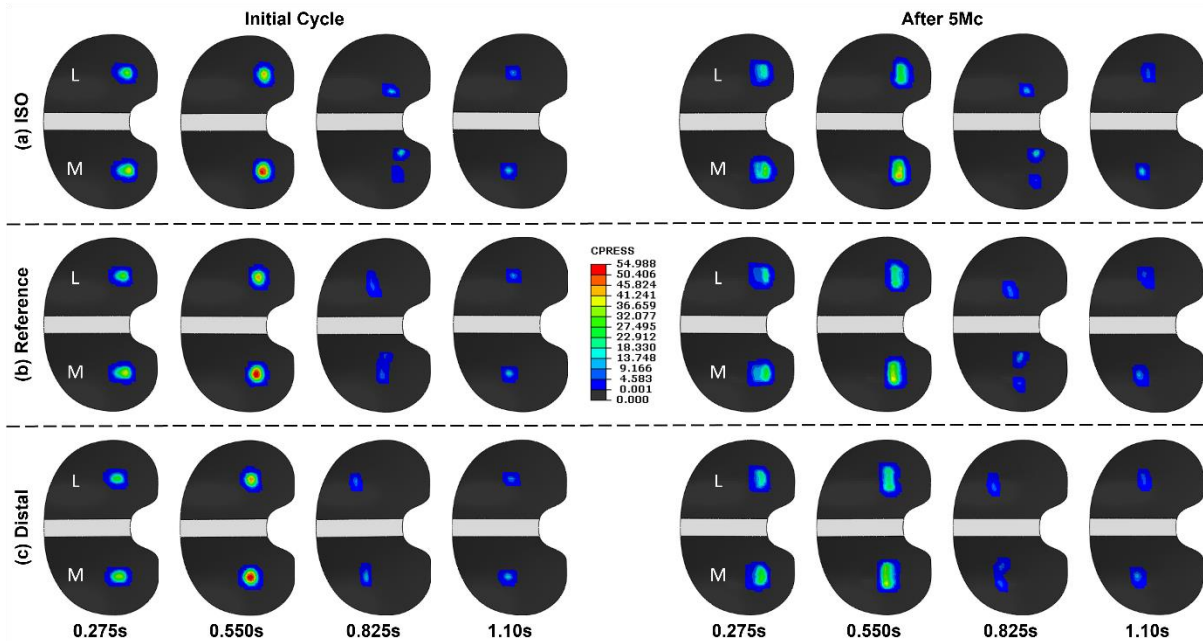
246

247

Figure 6 - Flowchart of Wear Algorithm

248 3. Results

249 Contact pressure trajectory and distribution over the gait cycle for the initial cycle and after 5Mc for
250 the polymeric insert are shown in Figure 7. The femoral CoR location changes the location of contact
251 pressure and thus the magnitude across the bearing surface. The maximum contact pressure is acting
252 on the medial side throughout the cycle, and for both the initial and after 5Mc. The legend for all
253 contour plots in this figure has been set to the highest contact pressure for these increments and CoRs,
254 which was at the initial cycle at 0.550s for the reference CoR. The area of contact pressure increases
255 after 5Mc; however, the pressure decreases for all CoRs. In addition, the start of the cycle has higher
256 contact pressure and a larger area of contact than the end of the cycle, which coincides with the load
257 peaks of the gait cycle (Figure 4). The change of CoR also shows that contact pressure location moves
258 further anteriorly from ISO (Figure 7a), to reference (Figure 7b), to distal (Figure 7c) CoRs.

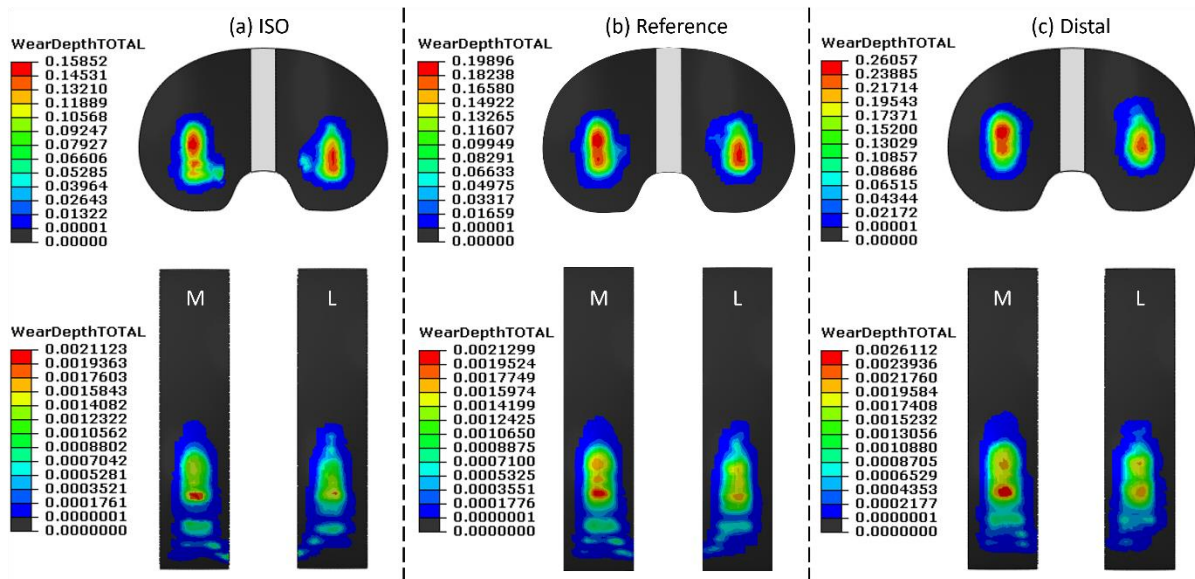


259

260 *Figure 7 – Polymeric Insert Contact Pressure Distribution for Initial Cycle (Left), and After 5Mc (Right) in MPa for (a) ISO, (b)*
 261 *Reference, and (c) Distal CoRs, where M = Medial and L = Lateral Sides*

262 Wear evolution after 5 Mc for the polymeric insert (top) and femoral (bottom) component at each of
 263 the femoral CoRs are shown in Figure 8. It can be seen that the maximum polymeric insert wear depth
 264 for ISO, reference, and distal CoRs are 0.16mm, 0.20mm, and 0.26mm respectively, whereas the
 265 maximum femoral wear depth is 2.11 μ m, 2.13 μ m, and 2.61 μ m respectively. For both components the
 266 maximum wear depth, red region, is located on the medial side, with the polymeric insert having a
 267 larger area of maximum wear depth than the femoral component. The wear pattern's location for
 268 both components is dependent on the femoral CoR, with ISO, Figure 8(a), being located more
 269 posteriorly, distal, Figure 8(c), more anteriorly, and reference, Figure 8(b), in between. With location
 270 of wear pattern changing in the AP direction, the polymeric insert wear pattern shape becomes more
 271 of an evenly distributed oval shape the further anteriorly the wear pattern is. This also coincides with
 272 the femoral component's region of minimal wear, for both medial and lateral condyles, between two
 273 regions of wear observed at the middle of the wear pattern. This minimum wear region can be seen
 274 clearly on the ISO CoR, Figure 8(a); however, it reduces further anteriorly the wear pattern is located.
 275 A minimal wear region is less noticeable but can also be seen on the medial side of the ISO polymeric
 276 insert wear pattern, Figure 8(a), but it is not visible for the other CoRs. In addition, the wear pattern
 277 on the medial side is positioned more posteriorly, and the lateral more anteriorly for both
 278 components.

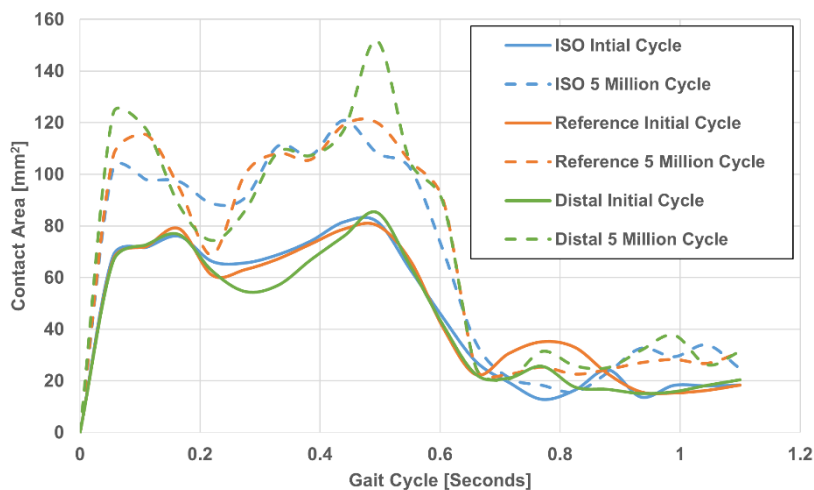
5 Million Cycles



279

280 *Figure 8 – Maximum Wear Depth for Polymeric Insert (Top) and Femoral Component (Bottom) in Millimetres After 5 Million*
 281 *Wear Cycles for (a) ISO, (b) Reference, and (c) Distal CoRs, where M = Medial and L = Lateral Sides*

282 After 5 Mc, the average polymeric insert-femoral component contact area across the gait cycle is
 283 different for each femoral CoR location, and changes significantly in comparison to the initial cycle,
 284 shown in Figure 9. The average contact area throughout the initial cycle was 46.55mm², 47.95mm²,
 285 44.86mm² for ISO, reference, and distal respectively. Whereas, after 5 Mc the average contact area
 286 was 66.53mm², 68.35mm², and 71.21mm² for ISO, reference, and distal respectively, with distal having
 287 around 7% more contact area than ISO. Throughout the gait cycle, the polymeric insert-femoral
 288 component contact area after 5 Mc is higher than the initial cycle for all CoRs, however at 0.7-0.9s the
 289 reference CoR initial cycle has the highest contact area than all 5 Mc CoRs.



290

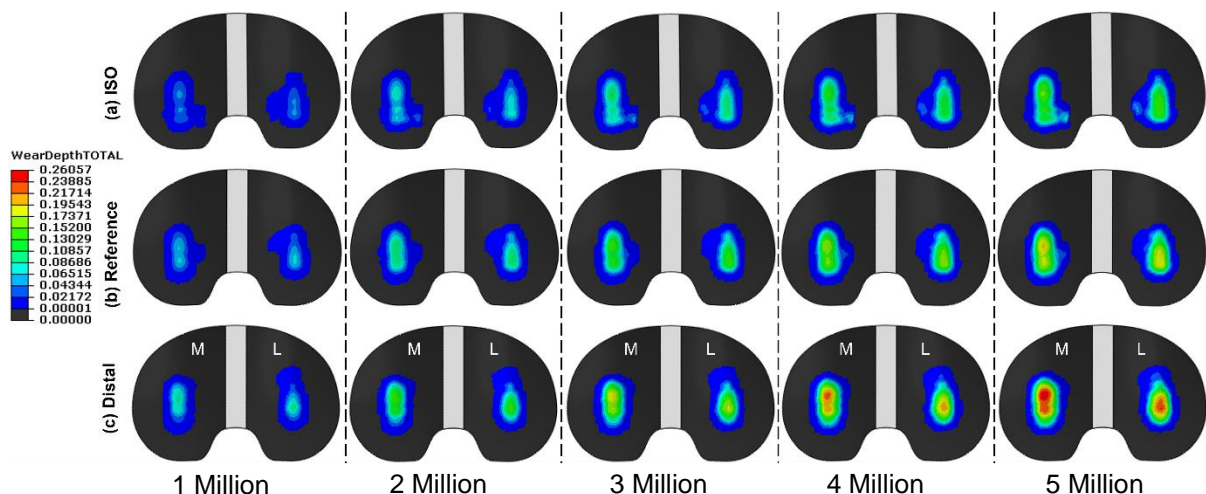
291 *Figure 9 – Polymeric Insert-Femoral Component Contact Area for Initial and 5 Million Cycles for all CoRs*

292 Figure 10 shows how the wear depth evolves on the polymeric insert, and Figure 11 for the femoral
 293 component over 5 Mc for each CoR. Both wear contours have a limit set to the distal CoR since it has
 294 the highest wear depth value, this allows for a visible comparison on how location of femoral CoR
 295 affects the wear evolution on the bearing surfaces. The wear pattern on both components enlarges in
 296 both the medial-lateral and AP direction over the 5 Mc for all CoRs.

297 One observation is that there is a clear difference between each of the CoR polymeric insert’s wear
 298 results, and that the ISO CoR wear, Figure 10(a), has just over half of the amount of the maximum
 299 polymeric insert’s distal CoR wear depth, Figure 10(c), distributed over the wear pattern. Observing
 300 the distribution of PE wear from 1-5 Mc for ISO CoR, Figure 10(a), it can be seen that a region of wear
 301 develops on the insides of the bearing surfaces. This becomes more prevalent after 2 Mc and starts to
 302 merge onto the main wear pattern after 3 Mc and 5 Mc on the medial and lateral sides respectively.
 303 As for the femoral wear distribution over 5 Mc for ISO CoR, Figure 11(a), the formation of the minimal
 304 region of wear can be seen after 1 Mc on the medial condyle, 2 Mc on the lateral, and becomes more
 305 significant over the 5 Mc.

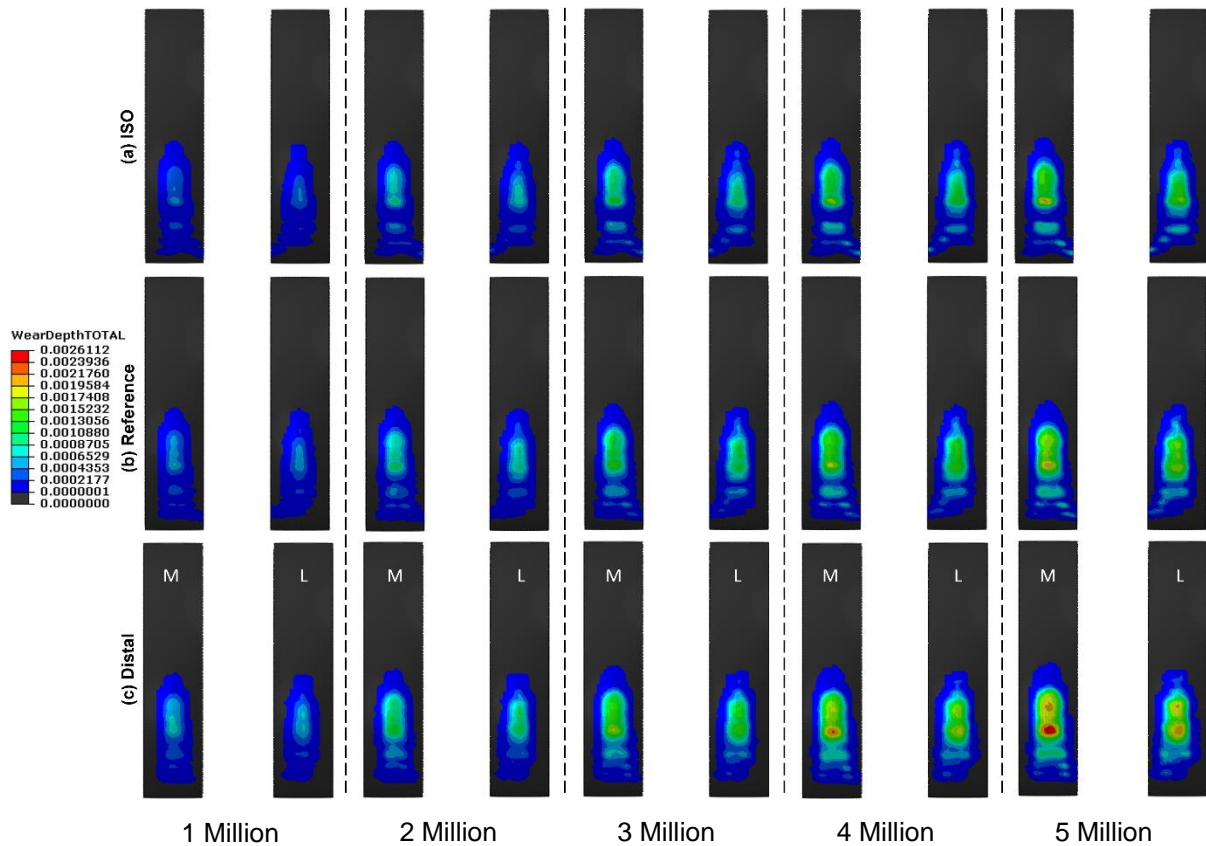
306 For the reference CoR polymeric insert’s wear distribution, Figure 10(b), the region of wear that
 307 develops on the insides of the bearing surface is more anteriorly than ISO CoR, Figure 10(a), and has
 308 a lower magnitude of wear depth. This region of wear becomes more prevalent on the medial side
 309 after 4 Mc. In addition, it can be seen that the wear evolution distributed over the bearing surface at
 310 the reference CoR, Figure 10(b), is more similar to the ISO CoR, Figure 10(a), with the only noticeable
 311 difference being the small area of maximum wear depth (yellow on contour plot) showing on the
 312 medial and lateral sides. This observation is also the same for the femoral reference CoRs wear
 313 pattern, Figure 11(b), in particularly the wear at the posterior side of both condyles being more similar
 314 to the ISO wear pattern, Figure 11(a), than the distal CoR, Figure 11(c).

315 The polymeric insert’s distal CoR wear pattern, Figure 10(c), shows that the wear depth values at 1 Mc
 316 is similar to the wear seen at the reference, Figure 10(b), and ISO, Figure 10(a), CoR at 2 Mc and 3 Mc
 317 respectively. This relationship is seen throughout the 5 Mc, where the distal CoR has similar wear
 318 depth value to reference and ISO CoRs that are 1 and 2 Mc further ahead respectively. The distal CoR
 319 polymeric insert wear pattern does not have a noticeable region of wear on the insides of the bearing
 320 surfaces forming over the 5 Mc. The distal CoR femoral component wear depth values, Figure 11(c),
 321 at 4 Mc is most similar to the wear at 5 Mc for both ISO, Figure 11(a), and reference CoRs, Figure 11(b),
 322 as they all show a dot of maximum wear depth on the medial condyle. Hence the relationship
 323 throughout the 5 Mc for the femoral distal CoR, Figure 11(c), has a similar wear depth value to the
 324 refence and ISO CoRs that are 1 Mc further ahead.



325

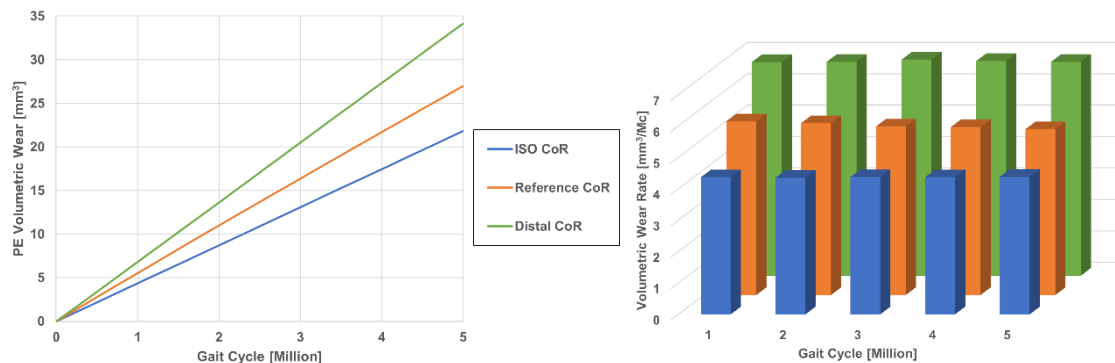
326 *Figure 10 – Polymeric Insert Wear Depth in Millimetres Over 5 Million Cycles for (a) ISO, (b) Reference, and (c) Distal CoRs,*
 327 *where M = Medial and L = Lateral Sides*



328

329 *Figure 11 – Femoral Wear Depth in Millimetres Over 5 Million Cycles for (a) ISO, (b) Reference, and (c) Distal CoRs, where M*
 330 *= Medial and L = Lateral Sides*

331 Volumetric wear and wear rates over the 5 Mc for the polymeric insert at each CoR are shown in Figure
 332 12. With the total volumetric wear after 5 Mc for ISO, reference, and distal CoR being 21.83mm³,
 333 27.00mm³, and 34.14mm³, which has an average wear rate over the 5 Mc of 4.37mm³/Mc,
 334 5.40mm³/Mc, and 6.83mm³/Mc respectively.



335

336 *Figure 12 – PE Volumetric Wear (Left), Volumetric Wear Rate (Right) Over 5 Million Cycles*

337 For the femoral component, the volumetric wear and wear rates over the 5 Mc at each CoR are shown
 338 in Figure 13. With the total volumetric wear after 5 Mc for ISO, reference, and distal CoR being
 339 0.21mm³, 0.27mm³, and 0.34mm³, which has an average wear rate over the 5 Mc of 0.04mm³/Mc,
 340 0.05mm³/Mc, and 0.07mm³/Mc respectively.

341

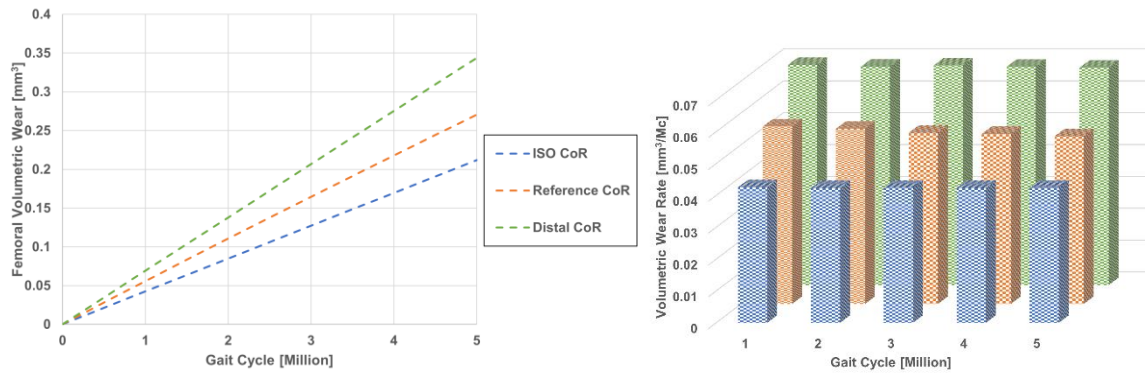


Figure 13 - Femoral Volumetric Wear (Left), Volumetric Wear Rate (Right) Over 5 Million Cycles

342

343

344 The volumetric wear for the polymeric insert increases by around 23.67% and 26.47% for ISO to
 345 reference and reference to distal CoR respectively, whereas the femoral component volumetric wear
 346 increases by around 27.61% and 26.98% respectively. A linear relationship between number of cycles
 347 and volumetric wear for all CoRs for both polymeric insert and femoral component are shown in Figure
 348 12 and Figure 13 respectively.

349 4. Discussion

350 The developed FE wear model has both components modelled as deformable bodies, and thus the
 351 addition of analysing femoral wear is possible. Metallic wear is an important factor to consider since
 352 metal debris from the femoral component and tibial tray can cause metallosis (Willis-Owen, Keene
 353 and Oakeshott, 2011; Arnholt et al., 2016), which can lead to further development of osteolysis
 354 (Kretzer et al., 2014; Marsh, Chamorro and Chatzistavrou, 2019), and thus contributes to TKR failure
 355 (Willis-Owen, Keene and Oakeshott, 2011; Sahan and Anagnostakos, 2020). Investigating femoral
 356 wear can help to further understand the wear evolution at the bearing surface of TKRs during its *in-*
 357 *vivo* lifespan.

358 As there are currently two types of wear testing standards that can be used to analyse wear, the force-
 359 controlled ISO 14243-1 (2009), and the more recent displacement-controlled ISO 14243-3 (2014),
 360 variations in wear results are expected and can be seen in literature (Table 3). A comparison of the
 361 two setups were investigated by Abdelgaied, Fisher and Jennings (2022), which resulted in predicted
 362 wear rates of more than double for the force-controlled setups. This relationship can be seen in results
 363 published in literature (Table 3). In addition, past ISO standards have alterations to gait cycles where
 364 AP motion and tibial rotation are flipped, positive being negative and negative being positive. This
 365 affects the evolution of wear, thus making comparisons with past published data difficult (Mell et al.,
 366 2018). Hence when comparing results of the developed model in this study with literature, variations
 367 of ISO setup, different geometries of implant design, and femoral CoR are factors that need to be
 368 carefully considered as they can affect wear rates and patterns.

369 The range of our results depending on the CoR predicts a wear rate of 4.37–6.83mm³/Mc (ISO-distal
 370 CoR), which shows a similar trend to a study by Mell, Wimmer and Lundberg (2019), whose finding
 371 show a wear rate of around 4.1–5.6mm³/Mc (ISO-distal CoR). This study's volumetric wear results are
 372 in agreement with other published displacement-controlled studies (Table 3), both computational and
 373 experimental findings, that are in the range of 3.4–9.2mm³/Mc.

374 When analysing Kretzer et al. (2014) knee simulator wear results, it can be determined that after 5 Mc
 375 there was a release of 7.28mg/Mc and 0.50mg/Mc of GUR 1020 PE wear and CoCr28Mo6 femoral

376 wear respectively. Volumetric wear rates can be calculated, when assuming density of GUR 1020 PE
 377 and CoCr28Mo6 are 0.937mg/mm³ and 8.47mg/mm³ respectively. This will result in a wear rate for PE
 378 being 7.77mm³/Mc, and the femoral component being 0.06mm³/Mc. The metallic wear rate
 379 calculated are comparable with the femoral wear rates in our study (Figure 13), being in the range of
 380 0.04-0.07mm³/Mc.

381 The variation of our results in comparison to other displacement-controlled published data can be
 382 explained by different implant designs, whether they have more conforming geometry between the
 383 PE-CoCr bearing surface, different location of femoral CoR, and in addition for other FE studies, applied
 384 material properties, and “scaling factor” used. Several studies (Wang et al., 2018; Mell, Wimmer and
 385 Lundberg, 2020; Abdelgaied, Fisher and Jennings, 2022) use ISO femoral CoR location, which is an
 386 estimation of where the femoral component will be in contact with the polymeric insert’s bearing
 387 surface at 30° and 60° flexion to create the imaginary planes and contact normal lines. Therefore, the
 388 location of femoral CoR applied for the same implant can vary for each study, resulting in an error
 389 margin and a variation in wear results.

390 In addition to knee simulator and FE studies, polymeric inserts from patients have been analysed to
 391 determine *in-vivo* wear through equipment such as coordinate-measuring machines (CMMs) (Pourzal
 392 et al., 2016; Knowlton, Bhutani and Wimmer, 2017; Bhalekar et al., 2021). With the use of CMMs,
 393 Bhalekar et al. (2021) determined volumetric wear for 76 contemporary inserts from four different
 394 manufacturers with a mean of 3.3 years *in-vivo*, which resulted in a median (IQR) volumetric wear rate
 395 of 9mm³/year (5 to 16). Knowlton, Bhutani and Wimmer (2017) investigated 51 TKRs, all the same
 396 implant design, and the results showed a wear rate of 12.9mm³/year. A focused study by Pourzal et
 397 al. (2016) determined the wear rate of 13 “normally wearing” (no delamination) inserts of the same
 398 design, with a mean of 6 years *in-vivo*, had a wear rate of 17mm³/year. Implants that have been
 399 retrieved and analysed can have varying wear rates, this can be due to numerous factors such as
 400 patient age, varying manufacturers and design of implant, and material combinations. The *in-vivo*
 401 wear rates are much higher than our study, assuming one Mc is approximately one year walking
 402 (Schmalzried et al., 1998), then our study predicts a wear rate around 4.37–6.83mm³/year depending
 403 on location of femoral CoR. The FE model is expected to predict a lower wear rate than the *in-vivo*
 404 rate as it only simulates walking on a level surface, thus it does not include more demanding activities
 405 of daily living that a TKR patient would experience, such as climbing and descending stairs, chair rising,
 406 sitting, and squatting as defined by Abdel-Jaber et al. (2015); (Dreyer et al., 2022). In addition, it is
 407 possible that the failed implants may have come from more active patients, those doing more than
 408 one million steps per year.

Study	Description	PE Wear Rate [mm ³ /Million Cycles]
Developed Model (Mell et al., 2022)	FE: ISO Displacement Controlled	4.37 – 6.83
	FE: ISO Displacement Controlled	4.50
	FE: ISO Force Controlled	8.60
(Abdelgaied, Fisher and Jennings, 2022)	Experimental Study: Leeds Gait Displacement Controlled	5.02 +/- 2.10
(Mell, Wimmer and Lundberg, 2020)	FE: ISO Displacement Controlled	4.45
(Wang et al., 2019)	FE: ISO Force Controlled	13.64
(Koh et al., 2019)	FE: Force Controlled	16.70-23.20

	Experimental: Force Controlled	17.80
(Wang et al., 2018)	FE: ISO Displacement Controlled	8.12
(Brockett et al., 2018)	FE: ISO Displacement Controlled	3.40-8.70 (XLK – GVF Material)
	Experimental: ISO Displacement Controlled	6.70-9.20 (XLK – GVF Material)
(Abdelgaied, Fisher and Jennings, 2018)	FE: Displacement Controlled	4.50
	Experimental: Displacement Controlled	5.80 +/- 1.40
(Kang et al., 2017)	FE: ISO Force Controlled	24.90
	Experimental: ISO Force Controlled	23.40 +/- 2.40
(Kretzer et al., 2014)	Experimental: ISO Force Controlled	7.77

Table 3 – Wear Comparison with FE and Knee Simulator Results from Literature

409

410 When considering geometrical differences of the implants used in the other studies, a similar
411 relationship is shown for wear regions on the medial and lateral sides. Our findings of the medial side
412 having a higher maximum wear depth compared to the lateral side, shown in Figure 8 and Figure 10,
413 agree with other FE studies in literature (Kang et al., 2017; Mell, Wimmer and Lundberg, 2019; Wang
414 et al., 2019; Koh et al., 2020), which is due to there being a greater load acting on the medial side from
415 the loading being offset medially (Knight et al., 2007). In addition, our study shows that there is a
416 natural rotation of the wear pattern with the medial side being offset more posteriorly compared to
417 the lateral being more anteriorly, which has also been observed in other FE studies (Kang et al., 2017;
418 Koh et al., 2019; Mell, Wimmer and Lundberg, 2019). These two observations for maximum wear
419 depth and rotation of wear pattern have also been seen in retrieval implants (Pourzal et al., 2016;
420 Knowlton, Bhutani and Wimmer, 2017). Furthermore, the relationship between the three CoRs and
421 how it affects wear depth, Figure 8, and volumetric wear, Figure 12, with ISO having the lowest, distal
422 the highest, and reference in the middle was also comparable with the findings of Mell, Wimmer and
423 Lundberg (2019). Also, their findings are comparable with our study with how the choice of femoral
424 CoR changes the location of the wear pattern, with ISO CoR having a wear pattern located posteriorly,
425 and then reference and distal CoR having a wear pattern that moves more anteriorly, as shown in
426 Figure 8 and Figure 10. This relationship is observed on the femoral components wear pattern as well,
427 Figure 11. Differences in sizes of wear patterns will be due to the variation of the implant investigated,
428 hence different designs and sizes, and thus conformity.

429 In our study, the comparison of the three CoRs wear pattern on the polymeric insert, Figure 10, shows
430 that the distal CoR has more of an evenly distributed oval shape wear pattern than the other CoRs.
431 This is due to there being less PE wear developing on the inside radius of the medial and lateral bearing
432 surface. This inside wear is prevalent on the ISO CoR study due to the femoral component articulating
433 more on the polymeric insert's posterior radius than the anterior radius during the gait cycle. The
434 polymeric insert's posterior and inner radius is more conforming to the femoral component than the
435 polymeric insert's anterior and outer radius, hence the region of wear occurring on the insides of the
436 polymeric insert's bearing surface. This reduces the further the wear pattern moves anteriorly; thus,
437 this wear region reduces at the reference and distal CoRs.

438 For both condyles, a region of minimal wear in between two wear regions at the middle of the femoral
439 wear pattern occurs for the ISO CoR and reduces further anteriorly the wear pattern is, shown in Figure

440 11. This shows that the ISO CoR has a less evenly distributed wear pattern evolution along the bearing
441 surface in comparison to the distal CoR. The femoral component also has an additional wear region
442 on the posterior of both condyles that forms a “V” shape at the ISO CoR if you put the two condyles
443 together, which also reduces further anteriorly the wear pattern is (Figure 11). This posterior wear
444 and the region of minimal wear on the femoral component seems to be linked to the polymeric insert’s
445 wear that occurs on the inside of the bearing surfaces, as they all reduce further anteriorly the wear
446 pattern is, and hence for both components an evenly distributed wear pattern is observed at the distal
447 CoR.

448 Contact area over the duration of the gait cycle on the PE-CoCr bearing surface (Figure 9), show a very
449 similar trend to literature studies (Kang et al., 2017; Wang et al., 2019; Koh et al., 2020; Abdelgaied,
450 Fisher and Jennings, 2022). Our contact area graphs look the most similar to Kang et al. (2017), the
451 other studies have a much greater contact area than what our study shows, with the most likely reason
452 being the implants investigated having a higher conformity. Overall, the trend of two main peaks
453 around 20% and 50% and then the trough plateauing after 60% of the cycle is comparable with
454 literature findings. The relationship of the peaks and troughs in contact area are very similar to the
455 axial load peaks and troughs through the gait cycle seen in Figure 4. The usual relationship in this study
456 of ISO having the smallest, then reference, and then distal having the highest for the wear results is
457 also the case for total contact area at the PE-CoCr bearing surface after 5 Mc. With the total polymeric
458 insert-femoral component contact area of our FE model being comparable to literature, this gives
459 confidence that the created geometry replicates that of a commercial TKR since this model’s geometry
460 was based of dimensions found in literature from Walker, Lowry and Kumar (2014).

461 The previous bespoke wear algorithm used for studies on THRs, required further development due to
462 the geometric nature of TKRs. The difference between the two implants meant that for each
463 increment of the walking cycle, the bearing surface of THRs are mostly conforming, whereas the
464 polymeric insert-femoral component of TKRs is less conforming in comparison. Essential changes were
465 made to ensure all nodes on the bearing surface between the polymeric insert and femoral
466 component have been paired together, hence the ‘1 to 3 pairing’ method used. In addition, a new
467 function was developed in the algorithm to gather the wear direction of each node on the polymeric
468 insert and femoral bearing surface. The wear direction was determined using the nodes’ “normal
469 direction”, which was extracted from the components’ geometry in the assembly interface of Abaqus
470 before an analysis was performed. Originally, ‘contact tangential resultant direction’ of each node at
471 the initial position before loading was used to determine this direction, which are generated for the
472 nodes that are in contact and can only be extracted once a single cycle is completed. This method
473 worked for a THR as the acetabular cup and the femoral head are either fully or almost fully
474 conforming (Kuster et al., 2000), hence a minute radial mismatch between the components of around
475 0.01-0.1mm (Li et al., 2020), whereas it would not be feasible for a TKR as the PE-CoCr bearing surface
476 has decreased conformity (Sivananthan, Goodman and Burke, 2014) with radial mismatch being in the
477 tens to hundreds of millimetres (Walker, Lowry and Kumar, 2014). This would mean that the majority
478 of nodes would not generate a contact tangential direction, and hence have no direction for wear to
479 be applied.

480 Currently this FE model is limited to bearing surface wear and does not simulate wear on the other
481 two interacting surfaces that a TKR would experience, wear between the backside of the polymeric
482 insert and the tibial tray (Holleyman et al., 2015), and the wear between the patella and the femoral
483 component (Huang et al., 2014). In addition, a fixed friction and wear coefficient has been used in this
484 study, which in reality can vary during the implant’s lifecycle.

485 5. Conclusion

486 The FE model and further developed bespoke wear algorithm presented in this study can accurately
487 predict bearing surface wear on both the polymeric insert and femoral component for millions of
488 cycles, in accordance with ISO 14243-3 (2014). With the computational wear method using Archard's
489 wear law, an approximate mesh size of 1mm for each component, and β of 100,000, has produced the
490 highest quality wear pattern on the PE-CoCr bearing surface. This method provides an insight into how
491 much polymeric and femoral wear debris is released from the bearing surface during the implant's
492 lifecycle in a computationally efficient time, with results that are validated to current published
493 computational, experimental, and retrieval findings.

494 The study showed that there is a wide range of wear values for different locations of femoral CoR,
495 with distal CoR having the most wear with an evenly distributed wear pattern, and ISO CoR having the
496 least wear with a less evenly distributed wear pattern in comparison. As such the location of femoral
497 CoR should be carefully considered as a factor that can affect wear results when performing any wear
498 investigation, whether *in-vivo*, *in-vitro*, and *in-silico*; and when investigating other activities of daily
499 living (Dreyer et al., 2022). Therefore, it needs to be ensured that the femoral CoR location is
500 consistent for all studies being compared, as it should not be a variable as it can drastically affect the
501 wear pattern and volumetric wear results. Hence a distal CoR may be the best choice, for *in-vitro* and
502 *in-silico* wear testing, to eradicate the possibility of femoral CoR location being a variable; as it is a
503 fixed location not an estimation, which only varies depending on the implant's distal radius.

504 The FE models' wear results and total contact area at the polymeric insert-femoral component bearing
505 surface gives confidence that the FE geometry and the wear analysis accurately replicates a
506 commercial TKRs *in-vivo* walking motion and can be used as a basis for further parametric studies. This
507 wear model can be used to predict how other factors such as material combinations, implant design,
508 and surgical procedures such as malalignment influence wear evolution on TKRs.

509 **Acknowledgements**

510 This work is funded by the School of Engineering, Liverpool John Moores University, Liverpool, UK.

References

Abdel-Jaber, S., Belvedere, C., Leardini, A. and Affatato, S. (2015) Wear simulation of total knee prostheses using load and kinematics waveforms from stair climbing. *Journal of biomechanics*, 48 (14), 3830-3836.

Abdelgaied, A., Fisher, J. and Jennings, L.M. (2018) A comprehensive combined experimental and computational framework for pre-clinical wear simulation of total knee replacements. *Journal of the Mechanical Behavior of Biomedical Materials*, 78, 282-291.

Abdelgaied, A., Fisher, J. and Jennings, L.M. (2022) Understanding the differences in wear testing method standards for total knee replacement. *Journal of the Mechanical Behavior of Biomedical Materials*, 132, 105258.

Abdelgaied, A., Liu, F., Brockett, C., Jennings, L., Fisher, J. and Jin, Z. (2011) Computational wear prediction of artificial knee joints based on a new wear law and formulation. *Journal of biomechanics*, 44 (6), 1108-1116.

Archard, J.F. and Hirst, W. (1956) The wear of metals under unlubricated conditions. *Proceedings of the Royal Society of London. Series A. Mathematical and Physical Sciences*, 236 (1206), 397-410.

Arnholt, C.M., MacDonald, D.W., Malkani, A.L., Klein, G.R., Rimnac, C.M., Kurtz, S.M., Kocagoz, S.B. and Gilbert, J.L. (2016) Corrosion Damage and Wear Mechanisms in Long-Term Retrieved CoCr Femoral Components for Total Knee Arthroplasty. *The Journal of Arthroplasty*, 31 (12), 2900-2906.

Bayliss, L.E., Culliford, D., Monk, A.P., Glyn-Jones, S., Prieto-Alhambra, D., Judge, A., Cooper, C., Carr, A.J., Arden, N.K., Beard, D.J. and Price, A.J. (2017) The effect of patient age at intervention on risk of implant revision after total replacement of the hip or knee: a population-based cohort study. *Lancet (London, England)*, 389 (10077), 1424-1430.

Beard, D.J., Davies, L.J., Cook, J.A., MacLennan, G., Price, A., Kent, S., Hudson, J., Carr, A., Leal, J. and Campbell, H. (2019) The clinical and cost-effectiveness of total versus partial knee replacement in patients with medial compartment osteoarthritis (TOPKAT): 5-year outcomes of a randomised controlled trial. *The Lancet*, 394 (10200), 746-756.

Bhalekar, R.M., Nargol, M.E., Shyam, N., Nargol, A.V.F., Wells, S.R., Collier, R., Pabbruwe, M., Joyce, T.J. and Langton, D.J. (2021) Tibial tray debonding from the cement mantle is associated with deformation of the backside of polyethylene tibial inserts. *The Bone & Joint Journal*, 103-B (12), 1791-1801.

Brockett, C.L., Abdelgaied, A., Haythornthwaite, T., Hardaker, C., Fisher, J. and Jennings, L.M. (2016) The influence of simulator input conditions on the wear of total knee replacements: An experimental and computational study. *Proceedings of the Institution of Mechanical Engineers, Part H: Journal of Engineering in Medicine*, 230 (5), 429-439.

Brockett, C.L., Carbone, S., Fisher, J. and Jennings, L.M. (2018) Influence of conformity on the wear of total knee replacement: An experimental study. *Proceedings of the Institution of Mechanical Engineers. Part H, Journal of engineering in medicine*, 232 (2), 127-134.

Carr, A.J., Robertsson, O., Graves, S., Price, A.J., Arden, N.K., Judge, A. and Beard, D.J. (2012) Knee replacement. *The Lancet*, 379 (9823), 1331-1340.

Castagnini, F., Sudanese, A., Bordini, B., Tassinari, E., Stea, S. and Toni, A. (2017) Total Knee Replacement in Young Patients: Survival and Causes of Revision in a Registry Population. *The Journal of Arthroplasty*, 32 (11), 3368-3372.

Chacko Rajan, S., Bretcanu, O., Deehan, D.J. and Joyce, T.J. (2020) Retrieval analysis of two contemporary total knee designs: Influence of femoral component roughness and type of polyethylene. *Journal of the Mechanical Behavior of Biomedical Materials*, 104, 103620.

Dreyer, M.J., Trepczynski, A., Hosseini Nasab, S.H., Kutzner, I., Schütz, P., Weisse, B., Dymke, J., Postolka, B., Moewis, P., Bergmann, G., Duda, G.N., Taylor, W.R., Damm, P. and Smith, C.R. (2022) European Society of Biomechanics S.M. Perren Award 2022: Standardized tibio-femoral implant loads and kinematics. *Journal of biomechanics*, 141, 111171.

Drohat, P.C., Kiehl, D.M. and Mess, D.C.F. (2018) The effect of obesity on the outcome of total knee arthroplasties in arthritic patients. *Journal of Student Research*, 7 (2).

English, R., Ashkanfar, A. and Rothwell, G. (2015) A computational approach to fretting wear prediction at the head–stem taper junction of total hip replacements. *Wear*, 338, 210-220.

Evans, J.T., Walker, R.W., Evans, J.P., Blom, A.W., Sayers, A. and Whitehouse, M.R. (2019) How long does a knee replacement last? A systematic review and meta-analysis of case series and national registry reports with more than 15 years of follow-up. *The Lancet*, 393 (10172), 655-663.

Fitzpatrick, C.K., Maag, C., Clary, C.W., Metcalfe, A., Langhorn, J. and Rullkoetter, P.J. (2016) Validation of a new computational 6-DOF knee simulator during dynamic activities. *Journal of biomechanics*, 49 (14), 3177-3184.

Fregly, B.J., Sawyer, W.G., Harman, M.K. and Banks, S.A. (2005) Computational wear prediction of a total knee replacement from in vivo kinematics. *Journal of biomechanics*, 38 (2), 305-314.

Gao, J., Xing, D., Dong, S. and Lin, J. (2020) The primary total knee arthroplasty: a global analysis. *Journal of Orthopaedic Surgery and Research*, 15 (1), 190.

Holleyman, R.J., Scholes, S.C., Weir, D., Jameson, S.S., Holland, J., Joyce, T.J. and Deehan, D.J. (2015) Changes in surface topography at the TKA backside articulation following in vivo service: a retrieval analysis. *Knee Surgery, Sports Traumatology, Arthroscopy*, 23 (12), 3523-3531.

Huang, C.-H., Hsu, L.-I., Lin, K.-J., Chang, T.-K., Cheng, C.-K., Lu, Y.-C., Chen, C.-S. and Huang, C.-H. (2014) Patellofemoral kinematics during deep knee flexion after total knee replacement: a computational simulation. *Knee Surgery, Sports Traumatology, Arthroscopy*, 22 (12), 3047-3053.

Hussain, O., Saleem, S. and Ahmad, B. (2019) Implant materials for knee and hip joint replacement: A review from the tribological perspective. *IOP Conference Series: Materials Science and Engineering of Conference*.

ISO 14243-1 (2009) ISO 14243-1. In: (ed.) *Implants for surgery — Wear of total knee-joint prostheses, Part 1: Loading and displacement parameters for wear-testing machines with load control and corresponding environmental conditions for test*.

ISO 14243-3 (2014) ISO 14243-3. In: (ed.) *Implants for surgery — Wear of total knee-joint prostheses, Part 3: Loading and displacement parameters for wear-testing machines with displacement control and corresponding environmental conditions for test*.

Jevsevar, D.S. (2013) Treatment of Osteoarthritis of the Knee: Evidence-Based Guideline, 2nd Edition. *JAAOS - Journal of the American Academy of Orthopaedic Surgeons*, 21 (9), 571-576.

Julin, J., Jämsen, E., Puolakka, T., Konttinen, Y.T. and Moilanen, T. (2010) Younger age increases the risk of early prosthesis failure following primary total knee replacement for osteoarthritis: A follow-up study of 32,019 total knee replacements in the Finnish Arthroplasty Register. *Acta Orthopaedica*, 81 (4), 413-419.

Kandahari, A.M., Yang, X., Laroche, K.A., Dighe, A.S., Pan, D. and Cui, Q. (2016) A review of UHMWPE wear-induced osteolysis: the role for early detection of the immune response. *Bone research*, 4, 16014-16014.

Kang, K.-T., Son, J., Kim, H.-J., Baek, C., Kwon, O.-R. and Koh, Y.-G. (2017) Wear predictions for UHMWPE material with various surface properties used on the femoral component in total knee arthroplasty: a computational simulation study. *Journal of Materials Science: Materials in Medicine*, 28 (7), 105.

Kim, K.T., Lee, S., Ko, D.O., Seo, B.S., Jung, W.S. and Chang, B.K. (2014) Causes of failure after total knee arthroplasty in osteoarthritis patients 55 years of age or younger. *Knee surgery & related research*, 26 (1), 13-19.

Knight, L.A., Pal, S., Coleman, J.C., Bronson, F., Haider, H., Levine, D.L., Taylor, M. and Rullkoetter, P.J. (2007) Comparison of long-term numerical and experimental total knee replacement wear during simulated gait loading. *Journal of biomechanics*, 40 (7), 1550-1558.

Knowlton, C.B., Bhutani, P. and Wimmer, M.A. (2017) Relationship of surface damage appearance and volumetric wear in retrieved TKR polyethylene liners. *Journal of Biomedical Materials Research Part B: Applied Biomaterials*, 105 (7), 2053-2059.

Knowlton, C.B., Lundberg, H.J., Wimmer, M.A. and Jacobs, J.J. (2020) Can a gait-dependent model predict wear on retrieved total knee arthroplasty components? *The Bone & Joint Journal*, 102-B (6_Supple_A), 129-137.

Koh, Y.-G., Jung, K.-H., Hong, H.-T., Kim, K.-M. and Kang, K.-T. (2019) Optimal Design of Patient-Specific Total Knee Arthroplasty for Improvement in Wear Performance. *Journal of Clinical Medicine*, 8 (11).

Koh, Y.-G., Park, K.-M., Lee, H.-Y., Park, J.-H. and Kang, K.-T. (2020) Prediction of wear performance in femoral and tibial conformity in patient-specific cruciate-retaining total knee arthroplasty. *Journal of Orthopaedic Surgery and Research*, 15 (1), 24.

Kretzer, J.P., Reinders, J., Sonntag, R., Hagmann, S., Streit, M., Jeager, S. and Moradi, B. (2014) Wear in total knee arthroplasty—just a question of polyethylene? *International Orthopaedics*, 38 (2), 335-340.

Kuster, M.S., Horz, S., Spalinger, E., Stachowiak, G.W. and Gächter, A. (2000) The Effects of Conformity and Load in Total Knee Replacement. *Clinical Orthopaedics and Related Research*[®], 375, 302-312.

Lee, H.K., Kim, S.M. and Lim, H.S. (2022) Computational Wear Prediction of TKR with Flatback Deformity during Gait. *Applied Sciences*, 12 (7), 3698.

Li, G., Peng, Y., Zhou, C., Jin, Z. and Bedair, H. (2020) The effect of structural parameters of total hip arthroplasty on polyethylene liner wear behavior: A theoretical model analysis. *Journal of Orthopaedic Research*, 38 (7), 1587-1595.

Maag, C., Metcalfe, A., Cracaoanu, I., Wise, C. and Auger, D.D. (2021) The development of simulator testing for total knee replacements. *Biosurface and Biotribology*, 7 (2), 70-82.

Marsh, A.C., Chamorro, N.P. and Chatzistavrou, X. (2019) 15 - Long-term performance and failure of orthopedic devices. In: Pawelec, K. M. and Planell, J. A. (ed.) *Bone Repair Biomaterials (Second Edition)*. Woodhead Publishing. pp. 379-410.

Mell, S.P., Fullam, S., Wimmer, M.A. and Lundberg, H.J. (2018) Finite element evaluation of the newest ISO testing standard for polyethylene total knee replacement liners. *Proceedings of the Institution of Mechanical Engineers. Part H, Journal of engineering in medicine*, 232 (6), 545-552.

Mell, S.P., Wimmer, M.A., Jacobs, J.J. and Lundberg, H.J. (2022) Optimal surgical component alignment minimizes TKR wear – An in silico study with nine alignment parameters. *Journal of the Mechanical Behavior of Biomedical Materials*, 125, 104939.

Mell, S.P., Wimmer, M.A. and Lundberg, H.J. (2019) The choice of the femoral center of rotation affects material loss in total knee replacement wear testing – A parametric finite element study of ISO 14243-3. *Journal of biomechanics*, 88, 104-112.

Mell, S.P., Wimmer, M.A. and Lundberg, H.J. (2020) Sensitivity of total knee replacement wear to variability in motion and load input: A parametric finite element analysis study. *Journal of Orthopaedic Research*[®], 38 (7), 1538-1549.

Michael, J.W., Schlüter-Brust, K.U. and Eysel, P. (2010) The epidemiology, etiology, diagnosis, and treatment of osteoarthritis of the knee. *Dtsch Arztebl Int*, 107 (9), 152-162.

NJR (2023) National Joint Registry Annual Report. In: (ed.) *The National Joint Registry 20th Annual Report 2023*.

O'Brien, S., Luo, Y., Wu, C., Petrak, M., Bohm, E. and Brandt, J.M. (2013) Computational development of a polyethylene wear model for the articular and backside surfaces in modular total knee replacements. *Tribology International*, 59, 284-291.

Ozer, A. (2022) Computational wear of knee implant polyethylene insert surface under continuous dynamic loading and posterior tibial slope variation based on cadaver experiments with comparative verification. *BMC Musculoskelet Disord*, 23 (1), 871.

Pfitzner, T., Moewis, P., Stein, P., Boeth, H., Trepczynski, A., von Roth, P. and Duda, G.N. (2018) Modifications of femoral component design in multi-radius total knee arthroplasty lead to higher lateral posterior femoro-tibial translation. *Knee Surgery, Sports Traumatology, Arthroscopy*, 26 (6), 1645-1655.

Pourzal, R., Knowlton, C.B., Hall, D.J., Laurent, M.P., Urban, R.M. and Wimmer, M.A. (2016) How Does Wear Rate Compare in Well-functioning Total Hip and Knee Replacements? A Postmortem Polyethylene Liner Study. *Clin Orthop Relat Res*, 474 (8), 1867-1875.

Price, A.J., Alvand, A., Troelsen, A., Katz, J.N., Hooper, G., Gray, A., Carr, A. and Beard, D. (2018) Knee replacement. *The Lancet*, 392 (10158), 1672-1682.

Sahan, I. and Anagnostakos, K. (2020) Metallosis after knee replacement: a review. *Archives of Orthopaedic and Trauma Surgery*, 140 (11), 1791-1808.

Schmalzried, T.P., Szuszczewicz, E.S., Northfield, M.R., Akizuki, K.H., Frankel, R.E., Belcher, G. and Amstutz, H.C. (1998) Quantitative assessment of walking activity after total hip or knee replacement. *JBJS*, 80 (1), 54-59.

Scholes, S.C., Kennard, E., Gangadharan, R., Weir, D., Holland, J., Deehan, D. and Joyce, T.J. (2013) Topographical analysis of the femoral components of ex vivo total knee replacements. *Journal of Materials Science: Materials in Medicine*, 24 (2), 547-554.

Sivananthan, S., Goodman, S. and Burke, M. (2014) 11 - Failure mechanisms in joint replacement**Note: This chapter is an updated version of Chapter 12, from the first edition of Joint replacement technology, edited by P. A. Revell and published by Woodhead Publishing, 2008. In: Revell, P. A. (ed.) *Joint Replacement Technology (Second Edition)*. Woodhead Publishing. pp. 370-400.

Skou, S.T., Roos, E.M., Laursen, M.B., Rathleff, M.S., Arendt-Nielsen, L., Rasmussen, S. and Simonsen, O. (2018) Total knee replacement and non-surgical treatment of knee osteoarthritis: 2-year outcome from two parallel randomized controlled trials. *Osteoarthritis and Cartilage*, 26 (9), 1170-1180.

Toh, S.M.S., Ashkanfar, A., English, R. and Rothwell, G. (2021) Computational method for bearing surface wear prediction in total hip replacements. *Journal of the Mechanical Behavior of Biomedical Materials*, 119, 104507.

Vince, K. (2014) The problem total knee replacement: systematic, comprehensive and efficient evaluation. *The Bone & Joint Journal*, 96 (11_Supple_A), 105-111.

Walker, P.S. (2015) The design and pre-clinical evaluation of knee replacements for osteoarthritis. *Journal of biomechanics*, 48 (5), 742-749.

Walker, P.S., Lowry, M.T. and Kumar, A. (2014) The Effect of Geometric Variations in Posterior-stabilized Knee Designs on Motion Characteristics Measured in a Knee Loading Machine. *Clinical Orthopaedics and Related Research*[®], 472 (1), 238-247.

Wang, X.-H., Li, H., Dong, X., Zhao, F. and Cheng, C.-K. (2019) Comparison of ISO 14243-1 to ASTM F3141 in terms of wearing of knee prostheses. *Clinical Biomechanics*, 63, 34-40.

Wang, X.-H., Zhang, W., Song, D.-Y., Li, H., Dong, X., Zhang, M., Zhao, F., Jin, Z.-M. and Cheng, C.-K. (2018) The impact of variations in input directions according to ISO 14243 on wearing of knee prostheses. *PLOS ONE*, 13 (10), e0206496.

Willing, R. (2013) Wear Modeling in Artificial Knee Joints. In: Wang, Q. J. and Chung, Y.-W. (ed.) Boston, MA: Springer US. pp. 4039-4045.

Willis-Owen, C.A., Keene, G.C. and Oakeshott, R.D. (2011) Early metallosis-related failure after total knee replacement. *The Journal of Bone & Joint Surgery British Volume*, 93-B (2), 205-209.

Witjes, S., van Geenen, R.C.I., Koenraadt, K.L.M., van der Hart, C.P., Blankevoort, L., Kerkhoffs, G.M.M.J. and Kuijer, P.P.F.M. (2017) Expectations of younger patients concerning activities after knee arthroplasty: are we asking the right questions? *Quality of Life Research*, 26 (2), 403-417.

Wright-Walker, C.J. and LaBerge, M. (2013) Wear in Knee Prostheses: Differences Compared with the Hip. In: Wang, Q. J. and Chung, Y.-W. (ed.) Boston, MA: Springer US. pp. 4001-4007.